Chemical Engineering Journal 431 (2022) 134125

Contents lists available at ScienceDirect

Chemical Engineering Journal

journal homepage: www.elsevier.com/locate/cej

High-index facets exposed on metal–organic framework for boosting photocatalytic carbon dioxide reduction

Xiao-Mei Cheng [a,b], Xiao-Yu Zhang [a], Xiao-Yao Dao [a], Shi-Qing Wang [a], Jing Zhao [b,*], Wei-Yin Sun [a,*]

[a] Coordination Chemistry Institute, State Key Laboratory of Coordination Chemistry, School of Chemistry and Chemical Engineering, Nanjing National Laboratory of Microstructures, Collaborative Innovation Center of Advanced Microstructures, Nanjing University, Nanjing 210023, China
[b] State Key Laboratory of Coordination Chemistry, Chemistry and Biomedicine Innovation Center (ChemBIC), School of Chemistry and Chemical Engineering, Nanjing University, Nanjing 210023, China

ARTICLE INFO

Keywords:
High-index facets
NH_2-MIL-125(Ti)
Metal-organic frameworks
Carbon dioxide
Photocatalytic reduction

ABSTRACT

Facets exposed on metal–organic frameworks (MOFs) are considered to be responsible for the efficiency of photocatalytic CO_2 conversion. Here, NH_2-MIL-125(Ti) with exposed high-index {1 1 2} facets has been investigated in detail for photocatalytic CO_2 reduction. Compared with low-index facets, the high-index {1 1 2} facets exhibit superior activity for CO_2-to-CO and CO_2-to-CH_4 conversions, which are 33 and 31 times higher for CO and CH_4 productions than the {0 0 1}/{1 1 1} facets. The superior photocatalytic activity is attributed to the large CO_2 uptake, efficient photoexcitation, charge separation and migration behaviors of the NH_2-MIL-125(Ti) with exposing high-index facets. This study provides an effective strategy to develop MOFs catalysts via facet-engineering for targeted performance.

1. Introduction

Photocatalytic carbon dioxide (CO_2) conversion into high value-added carbonaceous fuels and chemicals represents a green and economical approach to relieve energy crisis and provides a potential option to reach carbon neutrality [1–7]. Typically, the photoreduction of CO_2 involves five main processes, including light absorption, separation of charge carriers, migration of electrons, adsorption and activation of CO_2 molecules, reduction of CO_2 [8]. However, the photocatalytic CO_2 conversion efficiency is severely restricted by the fast recombination of photogenerated charge carriers and low charge transfer behavior [9]. Therefore, it is essential to develop effective strategies to further improve the photocatalytic efficiency of photocatalysts.

Metal-organic frameworks (MOFs) are a class of crystalline porous materials constructed from tunable metal or metal cluster nodes and organic linkers. They have various applications such as gas storage and separation, sensing, energy storage and catalysis [10–14]. Particularly, MOFs can be regarded as promising photocatalysts for CO_2 conversion due to their large specific surface areas and CO_2 adsorption capacity [15–17]. However, most of the metal nodes of MOFs serving as the catalytic active sites are majorly buried inside the framework, which is not beneficial to the reduction reaction since the photocatalytic reaction is a typical surface catalytic reaction [18–21]. Therefore, it is necessary to rational design and tailor the photocatalysts. It has been reported that there are effective ways to achieve high catalytic activity through regulation of morphology, facets and surface of MOFs [22–25]. Recently, great efforts have been paid towards the investigation of facet-effect of MOFs on photocatalytic reactions [26–29]. In our previous work, we precisely controlled the ratios of {0 0 1} and {1 1 1} low-index facets exposed over NH_2-MIL-125(Ti), and found that the activity of CO_2 photoreduction is enhanced with a gradually increasing exposed proportion of {1 1 1} facets [30]. The results ensure that photocatalytic activity can be improved by regulating exposing facets [31]. However, in contrast to low-index facets, high-index facet-dependent photoreduction of CO_2 is barely discovered for MOFs.

Herein, we employ three types of NH_2-MIL-125(Ti) with exposing {0 0 1}/{1 1 1}, {0 0 1}/{1 1 1}/{0 1 0} and {0 0 1}/{1 1 1}/{1 1 2} facets as model catalysts to explore the high-index facets effect on the photocatalytic CO_2 reduction. NH_2-MIL-125(Ti) enclosed with high-index {1 1 2} facets shows the highest activity for CO_2-to-CO and CO_2-to-CH_4 conversions, which are 33 and 31 times higher than the one with {0 0 1}/

* Corresponding authors.
E-mail addresses: jingzhao@nju.edu.cn (J. Zhao), sunwy@nju.edu.cn (W.-Y. Sun).

https://doi.org/10.1016/j.cej.2021.134125
Received 13 October 2021; Received in revised form 6 December 2021; Accepted 9 December 2021
Available online 14 December 2021

{1 1 1} facets, respectively. The high-index {1 1 2} facets have a significant enhancement of photoreduction activity compared to the low-index facets, because it could effectively broaden the light absorption range, improve the photoexcitation efficiency, inhibit electron-hole recombination and accelerate charge carriers separation and migration of NH_2-MIL-125(Ti).

2. Experimental section

2.1. Synthesis of NH_2-MIL-125(Ti) with different facets

{0 0 1}/{1 1 1} facets (T000): 2-Aminoterephthalic acid (NH_2-BDC) (0.28 g, 1.55 mmol) was added into a mixed solvent of N,N-dimethylformamide (DMF) (7.5 mL) and methanol (MeOH) (2.5 mL) with ultrasonication, and then titanium tetraisopropanolate (TPOT) (0.3 mL) was added under ultrasonication for another 5 min. The mixture was transferred into a 30 mL Teflon-line steel autoclave and kept at 150 °C for 8 h. The yellow products were collected, washed with DMF and MeOH several times, and dried for 5 h at 80 °C under reduced pressure.

{0 0 1}/{1 1 1}/{0 1 0} facets (T010): DMF (9.0 mL) and MeOH (1.0 mL) form the mixed solvent. NH_2-BDC (0.37 g, 2.04 mmol) was added into the mixed solvent with sonication. Then, titanium butoxide (TBOT) (0.45 mL) and acetic acid (AA) (0.25 mL) were added with ultrasonication for another 5 min. The mixture was transferred into a 18 mL Teflon-line steel autoclave, and heated at 150 °C for 24 h. After that the procedure is the same as that for preparation of T000.

{0 0 1}/{1 1 1}/{1 1 2} facets (T112): NH_2-BDC (0.54 g, 2.48 mmol) was dispersed into a mixed solvent of DMF (9.0 mL) and MeOH (1.0 mL) with ultrasonication. Then, TBOT (0.25 mL) was added and ultrasonication for another 5 min. The mixture was transferred into a 18 mL Teflon-line steel autoclave, and heated at 150 °C for 72 h, followed by the same procedure as mentioned above.

2.2. Photocatalytic CO_2 reduction

Photocatalytic reduction of CO_2 was realized in CEL-SPH2N-D9 (CeAulight, China) with a condensate circulating water filter (4 °C) to prevent the photothermal effect. Each sample (5 mg) was dispersed in MeCN (15 mL) and water (1.0 mL) with triethanolamine (TEOA) (3 mL) as a sacrificial agent, ultrasonicated to produce a suspension, and transferred into the reaction cell with 4 cm in diameter. Pure CO_2 gas (80 kPa, 99.999%, Shangyuan Gas) was injected in a vacuum reaction system. The photocatalytic experiments were finished under an xenon arc lamp (300 W) with AM 1.5G filter. The gas products were detected and quantified by an on-line gas chromatography (GC-9860) equipped with an FID detector. All photocatalytic data were repeated at least three times.

2.3. Electrochemical measurements

The electrochemical impedance spectroscopy (EIS) and Mott-Schottky tests were performed on the Zahner electrochemical workstation with standard three-electrode system using photocatalyst-coated carbon cloth as working electrode, graphite rod and Ag/AgCl electrode as counter and reference electrode for EIS, respectively. Photocatalyst-coated glassy carbon, graphite rod and Ag/AgCl electrode were utilized respectively as working, counter and reference electrode for Mott-Schottky test. Na_2SO_4 solution (0.2 M) was used as the electrolyte. The electrochemical experiments of linear sweep voltammetry (LSV) curves were achieved on a CHI 730E electrochemical workstation in a standard three-electrode system with the photocatalyst-coated ITO as working electrode, graphite rod as counter electrode, and Ag/AgCl as reference electrode. 300 μL of catalyst inks above mentioned were dropped onto the ITO plate (1 cm^2), and the electrolyte is N_2– and CO_2-saturated 0.1 M $KHCO_3$ solution. And the scan rate is 1 mV/s.

2.4. Photoelectrochemical measurements

Transient photocurrent measurements were finished on CHI 730E electrochemical workstation using ITO plate (1 cm^2), graphite rod and Ag/AgCl electrode as working, counter and reference electrode, respectively. Na_2SO_4 solution is the electrolyte. The as-synthesized sample (2 mg) was added into Nafion (10 μL) and methanol (1.0 mL) mixed solution, and the working electrode was prepared by dropping the suspension (300 μL) onto the surface of an ITO plate (1 cm^2), dried at room temperature, and the photo-responsive signals of the samples were measured under chopped light at 0.5 V. Switch light at least 10 recycles.

3. Results and discussion

3.1. Characterization of catalysts

NH_2-MIL-125(Ti) samples with different morphologies and facets were achieved by regulating the volume ratio of solvent, the amount of modulator and reaction time (Fig. 1a). The recognition and definition of the facets are exhibited in Fig. S1, in contrast to the low-index facets, the high-index facets are generally represented by {*hkl*} Miller indices with a minimum requirement of at least one index greater than one. As shown in Fig. 1b, a well-defined truncated octahedron of NH_2-MIL-125(Ti) was obtained, set as T000. With the addition of acetic acid (AA) as modulator, four new square facets {0 1 0} are formed at the corners of the truncated octahedron, which is named T010 (Fig. 1c). Additionally, with the reaction times increased to 72 h, eight small triangles of high-index {1 1 2} facets emerged at the corners of the truncated octahedron as illustrated in Fig. 1d, which is donated as T112. Energy dispersive X-ray (EDX) spectroscopy mapping images of T000, T010 and T112 are shown in Fig. S2. Powder X-ray diffraction (PXRD) patterns, high-resolution X-ray photoelectron spectroscopy (HR-XPS) and Fourier transform infrared (FT-IR) spectra were employed to estimate the crystal phases, chemical state of surface atoms and functional groups for the as-synthesized NH_2-MIL-125(Ti). All PXRD diffraction patterns of these three samples show the same crystal structure with the calculated NH_2-MIL-125(Ti) (Fig. 1e) [32], which is also supported by the FT-IR spectral data (Fig. S3). XPS survey spectra are provided in Fig. S4 to characterize the chemical composition and elemental chemical states of these three samples. Ti, O, N and C were detected, and the HR-XPS spectra of Ti 2p exhibit two peaks around 464.7 and 458.9 eV, which represent Ti $2p_{1/2}$ and Ti $2p_{3/2}$ of Ti^{IV} for the Ti-oxo cluster (Ti-O_x) on the surface of NH_2-MIL-125(Ti), respectively (Fig. 1f) [33]. The above results indicate that the adjustment of facets in this synthetic system just changes the surface atomic exposure without altering the framework structure of NH_2-MIL-125(Ti). Furthermore, it is noteworthy that more Ti-O_x clusters are not only exposed on the {1 1 2} facets surface but also located in the inside channels compared with the {0 1 0} facets (Fig. S5). Therefore, T112 has the highest Ti atomic concentration as well as the stoichiometric ratio of Ti to ligand among these three samples (Table S1), suggesting that more active sites are exposed and more efficient photocatalytic activity can be expected for the sample T112.

3.2. Optical properties of catalysts

Considering the effect of electronic band structure on photocatalytic efficiency, UV–vis diffuse reflectance spectra (DRS) and Mott-Schottky plots were examined. As shown in Fig. 2a and Fig. S6, the NH_2-MIL-125(Ti) exhibits a broad absorption region, and the wavelength of light absorption has an obvious red shift with high-index {1 1 2} exposed. T112 shows an enhanced optical absorption ability compared with the T000 and T010 as well as the bulky NH_2-MIL-125(Ti) without facet tuning, demonstrating an increase of light absorption ability with exposing high-index {1 1 2} facets. The corresponding HOMO-LUMO gap is estimated based on the Tauc plots derived from the DRS and the gaps of as-synthesized NH_2-MIL-125(Ti) are calculated to be 2.73,

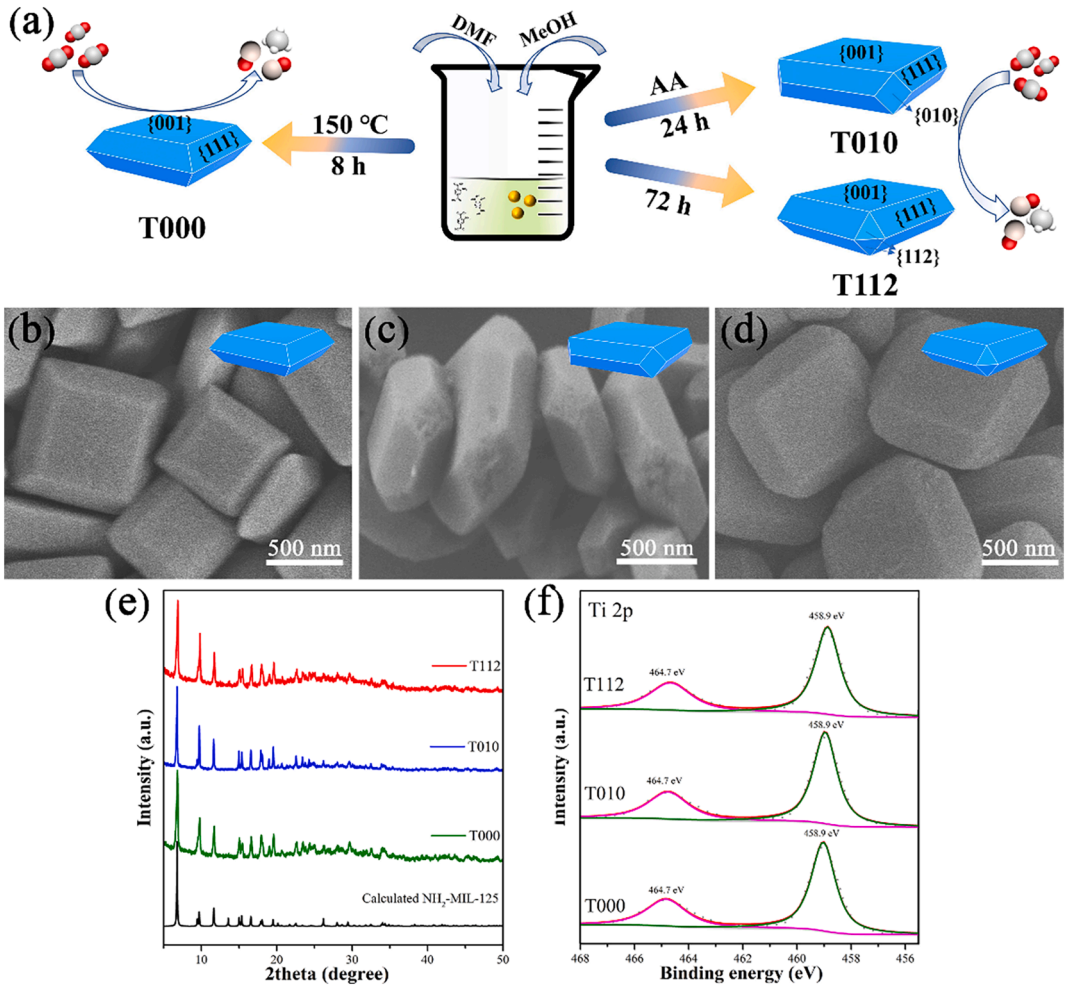

Fig. 1. Synthetic scheme (a) and SEM images of as-synthesized NH_2-MIL-125(Ti) with (b)T000, (c) T010 and (d) T112 facets. Scale bar: 500 nm. (e) PXRD patterns and (f) Ti 2p HR-XPS spectra of NH_2-MIL-125(Ti) with varied facets.

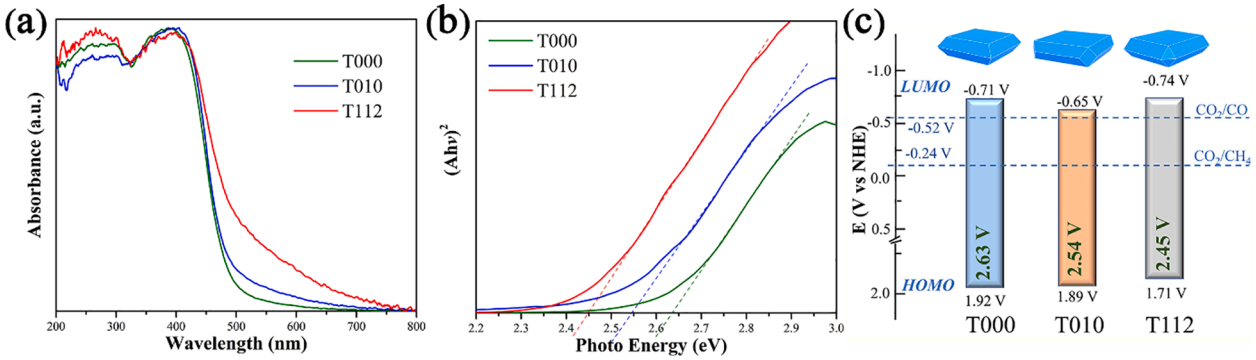

Fig. 2. (a) UV–vis diffuse reflectance spectra, (b) Tauc plots and (c) HOMO-LUMO gap of the T000, T010 and T112.

2.63, 2.54 and 2.45 eV for bulky sample, T000, T010 and T112, respectively (Fig. S6 and Fig. 2b). T112 possesses the smallest HOMO-LUMO gap, which means the lowest energy barrier to overcome for electron excitation from HOMO to LUMO level. It was reported that the LUMO level is contributed by the Ti 3p orbitals and O 2p orbitals while the HOMO level is composed of the O 2p orbitals [34]. Therefore, the regulation of facet could realize the modification and promotion of the NH_2-MIL-125(Ti)'s electronic band structure. The Mott-Schottky plots were employed to get the edges of the HOMO-LUMO gap of T000, T010 and T112 since the NH_2-MIL-125(Ti) is a typical n-type semiconductor (Fig. S7) [35]. And the flat potentials were determined to be −0.71, −0.65 and −0.74 V vs NHE for T000, T010 and T112 (Fig. 2c), respectively. The LUMO level potentials of these three samples are all above the potentials of CO_2-to-CO and CO_2-to-CH_4 conversions, which imply that the electronic band structures of these samples satisfy the thermodynamic requirement for CO_2-to-CO and CO_2-to-CH_4 reduction. T112 with exposing high-index {1 1 2} facets possesses the highest energy level of LUMO minimum, which could generate more reduction electrons to participate in the photocatalytic CO_2 reduction reaction.

3.3. Photocatalytic activity evaluation

After determining the facets and electronic band structures of three samples, photocatalytic CO_2 reduction activities were explored in the absence of additional photosensitizers. As shown in Fig. 3a, T112 exhibits superior photocatalytic activities with CO_2-to-CO and CO_2-to-CH_4 conversions, which are about 33 and 31 times higher than the yield of T000 with {001}/{111} facets, respectively (Table S2). The total apparent quantum yield (AQY) of T112 is 0.097% for the products of CO and CH_4, while the corresponding value of T000 is far below the T112, only 0.003% (Table S3). And the effectiveness of photo-electrons is remarkably enhanced with exposing {112} facets on the surface of NH_2-MIL-125(Ti). The effectiveness of photo-electrons of T112 is 100.46 μmol $g^{-1}h^{-1}$, about 32 times higher than the one of T000 (3.13 μmol $g^{-1}h^{-1}$) (Fig. 3c). While the CH_4 selectivity is comparable with value of 52.96%, 53.47% and 51.24% for T000, T010 and T112, respectively. The products of CO and CH_4 were quantified by gas chromatography with a FID detector (Fig. S8). No liquid product was detected by ^1H NMR spectrum (Fig. S9). In addition, the control experiments with different reaction conditions were also carried out (Fig. 3b). No CO and/or CH_4 were detected under different conditions, like without TEOA, without photocatalyst, using N_2 to replace CO_2 and without light. The isotopic $^{13}CO_2$ tracking experiment certificates that the carbon source of CO and CH_4 originated from the CO_2 gas (Fig. S10), confirming that the high photocatalytic activity is not derived from the decomposition of frameworks. In this photocatalytic system, TEOA was oxidized during the catalytic process (Fig. S11) [36]. The solution color change upon the light irradiation is attributed to the transformation between Ti^{IV} and Ti^{III}, electron paramagnetic resonance (EPR) spectra were employed to confirm the existence of Ti^{III} under light irradiation (Fig. S12) [37]. T112 exhibits enhanced EPR signals compared with T000 and T010, indicating the enhanced charge transfer due to the high-index facets exposed. Moreover, the photocatalytic stability of T112 is confirmed after five recycles (Fig. 3d) of the photocatalytic CO_2 reduction experiments. The PXRD pattern (Fig. S13) and SEM images (Fig. S14) of the T112 sample after photocatalytic reactions have no obvious change compared with the fresh catalyst, indicating that the T112 possesses superior structure stability in the photocatalytic reaction.

3.4. Possible mechanism of photocatalytic CO_2 reduction

In general, photocatalytic activity could be affected by various factors such as CO_2 uptake capacity, electronic band structure and charge carriers transfer efficiency [38]. Accordingly, N_2 and CO_2 adsorption isotherms of these three samples were studied (Figs. S15-S17). T112 possesses the largest Brunauer-Emmett-Teller (BET) specific surface area of 1232.65 $m^2 g^{-1}$ and the highest CO_2 uptakes of 131.66 and 66.83 $cm^3 g^{-1}$ at 273 and 298 K, respectively. {112} facets occupy only a small part of the surface area of the NH_2-MIL-125 (Ti), but have major contribution to the CO_2 uptake since the sample with {112} facets has different surface chemistry of the internal structure as illustrated in Fig. S5. The adsorption enthalpy (Qst) was calculated by dual-site Langmuir modal according to the CO_2 uptake data of these samples (Figs. S18-S20) [39]. T112 shows the largest adsorption enthalpy (35.69 kJ mol^{-1}), confirming that the strongest affinity between CO_2 and catalyst [40]. The specific surface area, CO_2 uptake and adsorption enthalpy of these samples are listed in Table S4. The larger specific surface can provide more adsorption and activation sites for CO_2 molecules. The higher CO_2 uptake and larger adsorption enthalpy demonstrate stronger affinity between CO_2 substrate and T112 with exposing

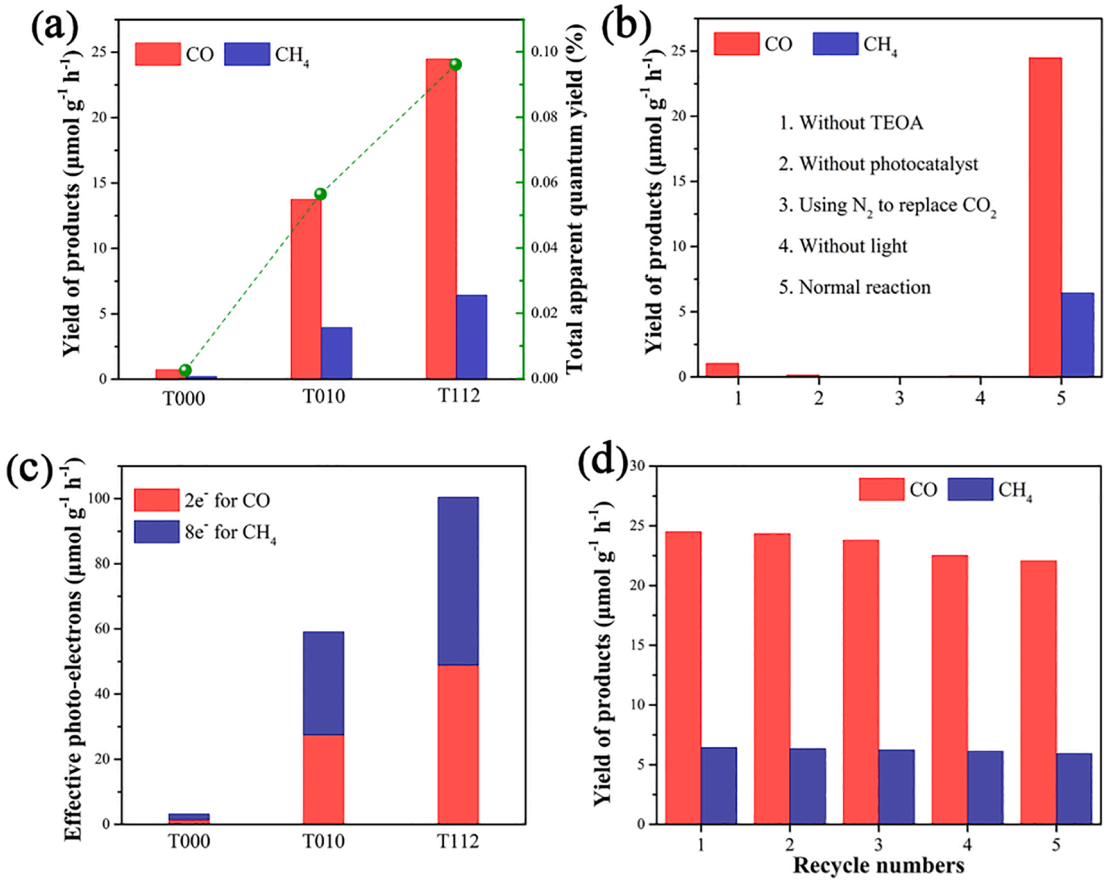

Fig. 3. (a) The yield of products and apparent quantum yield, (b) CO_2 reduction performance under varied conditions of T112, (c) the effective photo-electrons of CO and CH_4 after irradiation for 5 h of the T000, T010 and T112, (d) long-term stability tests of T112.

high-index {1 1 2} facets. CO_2 adsorption is the first step to determine the activity in the CO_2 photocatalytic reaction.

In addition, the separation and transfer of charge carriers is another key factor for CO_2 photoreduction. The steady-state photoluminescent (PL) and the time-resolved fluorescence decay experiments were measured to characterize photoelectronic properties. As shown in Fig. 4a, T000 shows a high PL intensity, indicating that the recombination of electron-hole pair. T112 exhibits a fast electron migration and separation efficiency with a low PL intensity. The obvious PL quenching reveals that the most rapid and efficient electron transfer occurs in T112 among these three NH_2-MIL-125(Ti) samples. The photogeneration carrier dynamics of the samples were explored by the time-resolved fluorescence decay experiments (Fig. 4b), and the fitting spectra were given in Fig. S21. The average carrier lifetime increases in the order of T000 (4.175 ± 0.085 ns) < T010 (4.474 ± 0.045 ns) < T112 (5.931 ± 0.085 ns). And the prolonged photoelectron lifetime of T112 is due to a lower recombination process, which allows more efficient photoelectron migration and separation, in well agreement with the steady-state PL results [41]. To elucidate the charge separation and migration efficiency of samples, the photoelectrochemical properties of the photocurrent transient response experiments were performed in five on–off cycles. The photocurrent intensity of T112 shows a significant enhancement compared with those of T000 and T010, manifesting the more effective charge migration occurred on the surface of T112 (Fig. 4c). The Nyquist plots from the electrochemical impedance spectroscopy (EIS) measurements further supported this judgment, where T112 exhibits the smallest radius, confirming the lowest charge transfer resistance (Rct) and the fastest interfacial charge transfer process (Fig. 4d). The electrochemical experiments of linear sweep voltammetry (LSV) curves were performed with a CO_2– and N_2-saturated atmosphere, respectively, to in-depth understand the catalytic activities among these samples (Fig. 4e) [42]. The results revealed that the current density under a CO_2 atmosphere is higher than those under N_2 atmosphere at the same potential. The onset potentials of T112 electrodes shift to a lower value compared with others in the CO_2 atmosphere. The onset potentials of these samples are in the order of T112 < T010 < T000. And the corresponding Tafel plots were calculated based on LSV curves of CO_2 reduction (Fig. 4f), T112 shows a minimum Tafel slope with a lower reduced kinetic barrier for CO_2 reduction [43]. The results indicate that the NH_2-MIL-125(Ti) with different facets exposed have different CO_2 photocatalytic reduction abilities, particularly the high-index {1 1 2} facets exposed in T112 have superior photocatalytic activity (Table S5).

Based on the above discussion, a possible mechanism concerning the superior photocatalytic CO_2 conversion performance of NH_2-MIL-125 (Ti) with exposing high-index facets was proposed (Fig. 5). The HOMO-

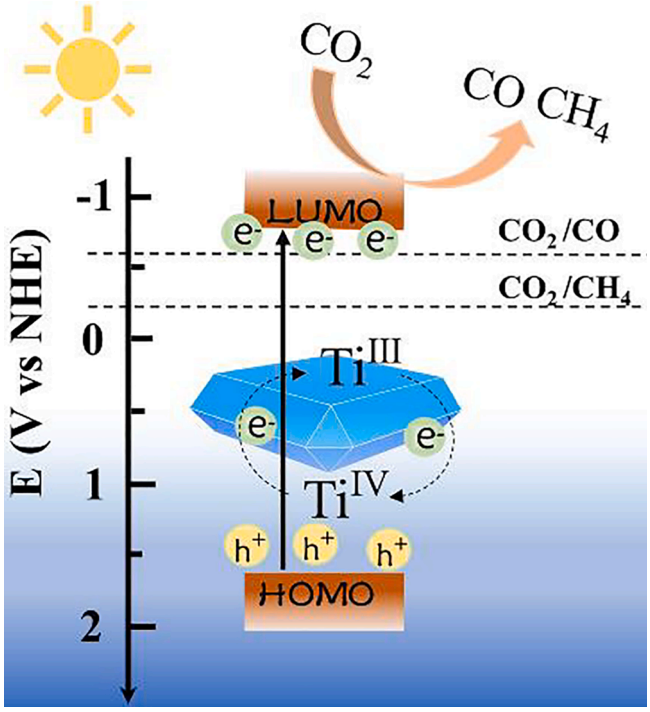

Fig. 5. Reaction scheme of T112 in photocatalytic CO_2 reduction.

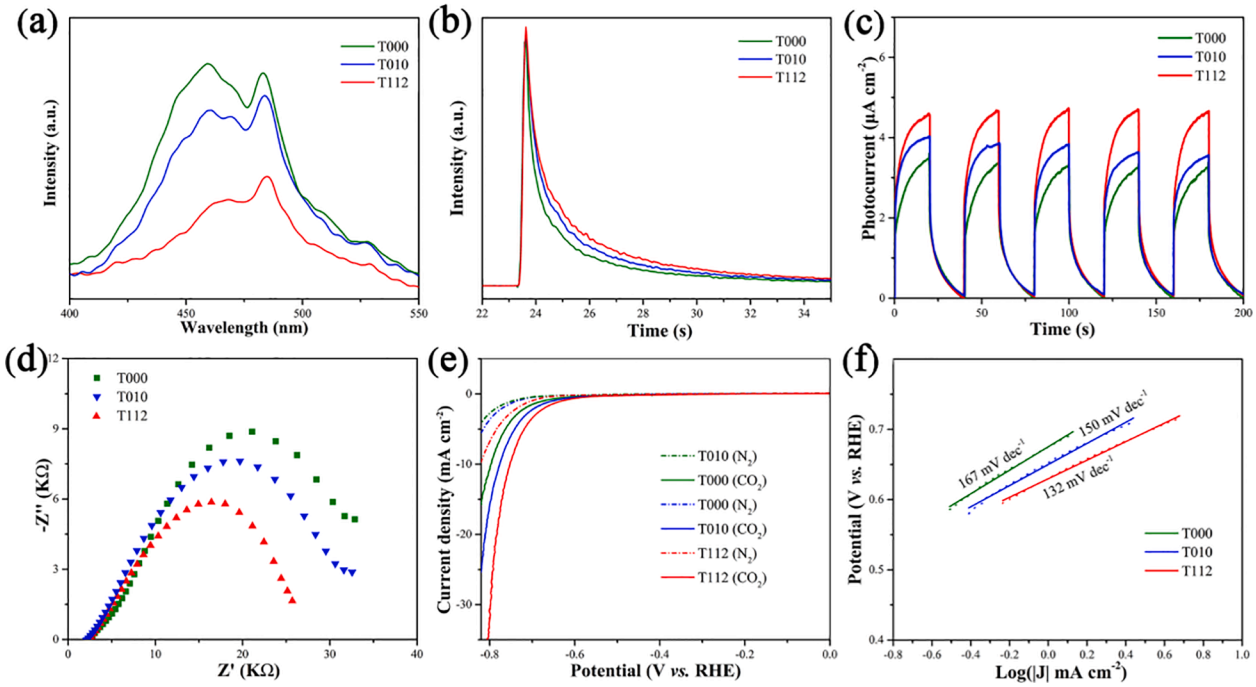

Fig. 4. (a) Steady-state PL spectra, (b) time-resolved fluorescence decay spectra, (c) photocurrent transient response, (d) EIS Nyquist plots, (e) LSV curves and (f) Tafel plots of CO_2 reduction for as-synthesized T000, T010 and T112.

LUMO gap can be adjusted by exposing the different facets, high-index facets exposed to show a narrow HOMO-LUMO gap in favor of the electrons photoexcited. While the low photoreduction activity of T000 with {001}/{111} facets exposed results from the electronic band structure, which is hard to generate electron by photoexcitation. Under simulated light irradiation, the electrons in the HOMO level were excited and the photoinduced electrons can be transferred to the LUMO level positions, which trigger the reduction reaction due to the appropriate value being higher than the value of CO_2-to-CO (−0.52 eV) and CO_2-to-CH_4 (−0.24 eV) conversion. Combined with the efficient active sites provided by high specific surface area and CO_2 adsorption, the CO_2 molecules are adsorbed on the surface and activated by the photoexcited electrons. Meanwhile, Ti^{IV} on the exposed facets of NH_2-MIL-125(Ti) was converted to Ti^{III} by capturing the electrons during the photocatalytic reaction process. And Ti^{III} sites have strong reducibility to realize the CO_2-to-CO and CO_2-to-CH_4 conversion. Hence, T112 with exposing the high-index facets acts as a more effective photocatalyst for CO_2 reduction by a synergy of more active sites and effectively charge separation and migration.

4. Conclusions

In summary, we successfully prepared three types NH_2-MIL-125(Ti) with {001}/{111}, {001}/{111}/{010} and {001}/{111}/{112} co-exposed mixture facets as model photocatalysts to investigate the facet-effect on photocatalytic CO_2 reduction. It was found that the NH_2-MIL-125(Ti) with exposing high-index {112} facets exhibits superior photocatalytic CO_2 activities for CO_2-to-CO and CO_2-to-CH_4 conversion. The improved photocatalytic activity can be attributed to the broad light absorption, promoted the CO_2 adsorption, enhanced the electron reduction ability and facilitated charge separation and transfer while exposing the high-index facets. The Ti atomic concentration on the catalyst surface is changed by regulating the facet exposed. And the transition between Ti^{IV} and Ti^{III} has been considered in the photoreaction, which accelerated the charge separation and migration and enhanced photocatalytic activity eventually. This work provides a promising strategy for improving photocatalytic activity by constructing active facets on MOFs for achieving facet engineering on photocatalytic application.

Declaration of Competing Interest

The authors declare that they have no known competing financial interests or personal relationships that could have appeared to influence the work reported in this paper.

Acknowledgements

We gratefully acknowledge the National Natural Science Foundation of China (grant no. 22171131) and the National Basic Research Program of China (grant no. 2017YFA0303504) for financial support of this work. This work was also supported by a Project Funded by the Priority Academic Program Development of Jiangsu Higher Education Institutions.

Appendix A. Supplementary data

Supplementary data to this article can be found online at https://doi.org/10.1016/j.cej.2021.134125.

References

[1] Y. Pan, Y. Qian, X. Zhang, S.-Q. Chu, Y. Yang, C. Ding, X. Wang, S.-H. Yu, H.-L. Jiang, Precise Fabrication of single-atom alloy co-catalyst with optimal charge state for enhanced photocatalysis, Natl. Sci. Rev. 8 (2021) nwaa224, https://doi.org/10.1093/nsr/nwaa224.

[2] S. Karmakar, S. Barman, F.A. Rahimi, T.K. Maji, Covalent grafting of molecular photosensitizer and catalyst on MOF-808: effect of pore confinement toward visible light-driven CO_2 reduction in water, Energy Environ. Sci. 14 (4) (2021) 2429–2440, https://doi.org/10.1039/D0EE03643A.

[3] W.D. Jones, Carbon capture and conversion, J. Am. Chem. Soc. 142 (11) (2020) 4955–4957, https://doi.org/10.1021/jacs.0c02356.

[4] I.I. Alkhatib, C. Garlisi, M. Pagliaro, K. Al-Ali, G. Palmisano, Metal-organic frameworks for photocatalytic CO_2 Reduction under visible radiation: review of strategies and applications, Catal. Today 340 (2020) 209–224, https://doi.org/10.1016/j.cattod.2018.09.032.

[5] W. Gao, S. Liang, R. Wang, Q. Jiang, Y.u. Zhang, Q. Zheng, B. Xie, C.Y. Toe, X. Zhu, J. Wang, L. Huang, Y. Gao, Z. Wang, C. Jo, Q. Wang, L. Wang, Y. Liu, B. Louis, J. Scott, A.-C. Roger, R. Amal, H. He, S.-E. Park, Industrial carbon dioxide capture and utilization: state of the art and future challenges, Chem. Soc. Rev. 49 (23) (2020) 8584–8686, https://doi.org/10.1039/D0CS00025F.

[6] X. Chang, T. Wang, J. Gong, CO_2 photo-reduction: insights into CO_2 activation and reaction on surfaces of photocatalysts, Energy Environ. Sci. 9 (7) (2016) 2177–2196, https://doi.org/10.1039/C6EE00383D.

[7] Y.A. Wu, I. McNulty, C. Liu, K.C. Lau, Q.i. Liu, A.P. Paulikas, C.-J. Sun, Z. Cai, J. R. Guest, Y. Ren, V. Stamenkovic, L.A. Curtiss, Y. Liu, T. Rajh, Facet-dependent active sites of a single Cu_2O particle photocatalyst for CO_2 reduction to methanol, Nat. Energy 4 (11) (2019) 957–968, https://doi.org/10.1038/s41560-019-0490-3.

[8] A. Meng, B. Cheng, H. Tan, J. Fan, C. Su, J. Yu, TiO_2/polydopamine S-scheme heterojunction photocatalyst with enhanced CO_2-reduction selectivity, Appl. Catal., B 289 (2021) 120039, https://doi.org/10.1016/j.apcatb.2021.120039.

[9] H. Zhang, T. Itoi, T. Konishi, Y. Izumi, Dual photocatalytic roles of light: charge separation at the band gap and heat via localized surface plasmon resonance to convert CO_2 into CO over SILVER-ZIRCONIUM Oxide, J. Am. Chem. Soc. 141 (15) (2019) 6292–6301, https://doi.org/10.1021/jacs.8b13894.

[10] C.A. Trickett, A. Helal, B.A. Al-Maythalony, Z.H. Yamani, K.E. Cordova, O. M. Yaghi, The chemistry of metal-organic frameworks for CO_2 capture, regeneration and conversion, Nat. Rev. Mater. 2 (2017) 17045, https://doi.org/10.1038/natrevmats.2017.45.

[11] S. Wang, X. Wang, Imidazolium ionic liquids, imidazolylidene heterocyclic carbenes, and zeolitic imidazolate frameworks for CO_2 capture and photochemical reduction, Angew. Chem. Int. Ed. 55 (7) (2016) 2308–2320, https://doi.org/10.1002/anie.201507145.

[12] Y.-B. Huang, J. Liang, X.-S. Wang, R. Cao, Multifunctional metal-organic framework catalysts: synergistic catalysis and tandem reactions, Chem. Soc. Rev. 46 (1) (2017) 126–157, https://doi.org/10.1039/C6CS00250A.

[13] X. Zhang, Z. Chen, X. Liu, S.L. Hanna, X. Wang, R. Taheri-Ledari, A. Maleki, P. Li, O.K. Farha, A historical overview of the activation and porosity of metal-organic frameworks, Chem. Soc. Rev. 49 (20) (2020) 7406–7427, https://doi.org/10.1039/D0CS00997K.

[14] K. Wang, Q. Li, Z. Ren, C. Li, Y. Chu, Z. Wang, M. Zhang, H. Wu, Q. Zhang, 2D metal-organic frameworks (MOFs) for high-performance BatCap hybrid devices, Small 16 (30) (2020) 2001987, https://doi.org/10.1002/smll.v16.3010.1002/smll.202001987.

[15] Y. Li, W.-S. Lo, F. Zhang, X. Si, L.-Y. Chou, X.-Y. Liu, B.P. Williams, Y.-H. Li, S.-H. Jung, Y.-S. Hsu, F.-S. Liao, F.-K. Shieh, M.N. Ismail, W. Huang, C.-K. Tsung, Creating an aligned interface between nanoparticles and MOFs by concurrent replacement of capping agents, J. Am. Chem. Soc. 143 (13) (2021) 5182–5190, https://doi.org/10.1021/jacs.1c01357.

[16] Y. Yan, C. Li, Y. Wu, J. Gao, Q. Zhang, From isolated Ti-oxo clusters to infinite Ti-oxo chains and sheets: recent advances in photoactive Ti-based MOFs, J. Mater. Chem. A 8 (31) (2020) 15245–15270, https://doi.org/10.1039/D0TA03749D.

[17] S.-Q. Wang, X.-Y. Zhang, X.-Y. Dao, X.-M. Cheng, W.-Y. Sun, Cu_2O@Cu@UiO-66-NH_2 ternary nanocubes for photocatalytic CO_2 reduction, ACS Appl. Nano Mater. 3 (10) (2020) 10437–10445, https://doi.org/10.1021/acsanm.0c02312.

[18] L. Liu, S. Wang, H. Huang, Y. Zhang, T. Ma, Surface sites engineering on semiconductors to boost photocatalytic CO_2 reduction, Nano Energy 75 (2020) 104959, https://doi.org/10.1016/j.nanoen.2020.104959.

[19] C. Xiao, B.-A. Lu, P. Xue, N. Tian, Z.-Y. Zhou, X. Lin, W.-F. Lin, S.-G. Sun, High-index-facet- and high-surface-energy nanocrystals of metals and metal oxides as highly efficient catalysts, Joule 4 (12) (2020) 2562–2598, https://doi.org/10.1016/j.joule.2020.10.002.

[20] R. M.s, S. Shanmuga Priya, N.C. Freudenberg, K. Sudhakar, M. Tahir, Metal-organic framework-based photocatalysts for carbon dioxide reduction to methanol: a review on progress and application, J. CO_2 Util. 43 (2021) 101374, https://doi.org/10.1016/j.jcou.2020.101374.

[21] X. Yuan, Q. Mu, S. Xue, Y. Su, Y. Zhu, H. Sun, Z. Deng, Y. Peng, Polypyrrole reinforced ZIF-67 with modulated facet exposure and billion-fold electrical conductivity enhancement towards robust photocatalytic CO_2 Reduction, J. Energy Chem. 60 (2021) 202–208, https://doi.org/10.1016/j.jechem.2020.12.025.

[22] R. Qin, N. Zheng, Catalysis selects its own favorite facets, Chem 5 (8) (2019) 1935–1937, https://doi.org/10.1016/j.chempr.2019.07.011.

[23] J. Wan, D. Liu, H. Xiao, H. Rong, S. Guan, F. Xie, D. Wang, Y. Li, Facet Engineering in metal organic frameworks to improve their electrochemical activity for water oxidation, Chem. Commun. 56 (31) (2020) 4316–4319, https://doi.org/10.1039/D0CC00700E.

[24] M. Wang, J. Liu, C. Guo, X. Gao, C. Gong, Y. Wang, B.o. Liu, X. Li, G.G. Gurzadyan, L. Sun, Metal-organic frameworks (ZIF-67) as efficient cocatalysts for photocatalytic reduction of CO_2: the role of the morphology effect, J. Mater. Chem. A 6 (11) (2018) 4768–4775, https://doi.org/10.1039/C8TA00154E.

[25] C. Li, H. Xu, J. Gao, W. Du, L. Shangguan, X. Zhang, R.-B. Lin, H. Wu, W. Zhou, X. Liu, J. Yao, B. Chen, Tunable titanium metal–organic frameworks with infinite 1D Ti–O rods for efficient visible-light-driven photocatalytic H_2 evolution,

J. Mater. Chem. A 7 (19) (2019) 11928–11933, https://doi.org/10.1039/C9TA01942A.
[26] K. Shen, L. Zhang, X.D. Chen, L.M. Liu, D.L. Zhang, Y. Han, J.Y. Chen, J.L. Long, R. Luque, Y.W. Li, B.L. Chen, Ordered macro-microporous metal-organic framework single crystals, Science 359 (2018) 206–210, https://doi.org/10.1126/science.aao3403.
[27] Z. Zhang, Y. Tao, H. Tian, Q. Yue, S. Liu, Y. Liu, X. Li, Y. Lu, Z. Sun, E. Kraka, S. Liu, Chelation-assisted selective etching construction of hierarchical polyoxometalate-based metal-organic framework, Chem. Mater. 32 (13) (2020) 5550–5557, https://doi.org/10.1021/acs.chemmater.0c00440.
[28] Y. Niu, Y. Yuan, Q. Zhang, F. Chang, L. Yang, Z. Chen, Z. Bai, Morphology-controlled synthesis of metal-organic frameworks derived lattice plane-altered iron oxide for efficient trifunctional electrocatalysts, Nano Energy 82 (2021) 105699, https://doi.org/10.1016/j.nanoen.2020.105699.
[29] W. Yang, H.-J. Wang, R.-R. Liu, J.-W. Wang, C. Zhang, C. Li, D.-C. Zhong, T.-B. Lu, Tailoring crystal facets of metal-organic layers to enhance photocatalytic activity for CO_2 reduction, Angew. Chem. Int. Ed. 60 (1) (2021) 409–414, https://doi.org/10.1002/anie.202011068.
[30] X.-M. Cheng, X.-Y. Dao, S.-Q. Wang, J. Zhao, W.-Y. Sun, Enhanced photocatalytic CO_2 reduction activity over NH_2-MIL-125(Ti) by facet regulation, ACS Catal. 11 (2) (2021) 650–658, https://doi.org/10.1021/acscatal.0c04426.
[31] S. Bera, R.K. Behera, N. Pradhan, Alpha-halo ketone for polyhedral perovskite nanocrystals: evolutions, shape conversions, ligand chemistry, and self-assembly, J. Am. Chem. Soc. 142 (2020) 20865–20874, https://doi.org/10.1021/jacs.0c10688.
[32] A.P. Smalley, D.G. Reid, J.C. Tan, G.O. Lloyd, Alternative synthetic methodology for amide formation in the post-synthetic modification of Ti-MIL125-NH_2, CrystEngComm 15 (45) (2013) 9368, https://doi.org/10.1039/c3ce41332b.
[33] S. Chen, G. Hai, H. Gao, X. Chen, A. Li, X. Zhang, W. Dong, Modulation of the charge transfer behavior of Ni(II)-doped NH_2-MIL-125(Ti): regulation of Ni ions content and enhanced photocatalytic CO_2 reduction performance, Chem. Eng. J. 406 (2021) 126886, https://doi.org/10.1016/j.cej.2020.126886.
[34] S.Y. Chen, F.C. Yang, H.Y. Gao, J.Y. Wang, X. Chen, X.W. Zhang, J. Li, A. Li, Constructure of dual ligand Ti-based MOFs with enhanced photocatalytic CO_2 reduction performance, J. CO_2 Util. 48 (2021), 101528, https://doi.org/10.1016/j.jcou.2021.101528.
[35] H.-Q. Xu, J. Hu, D. Wang, Z. Li, Q. Zhang, Y.i. Luo, S.-H. Yu, H.-L. Jiang, Visible-light photoreduction of CO_2 in a metal-organic framework: boosting electron-hole separation via electron trap states, J. Am. Chem. Soc. 137 (42) (2015) 13440–13443, https://doi.org/10.1021/jacs.5b08773.
[36] H. Zhang, J. Wei, J. Dong, G. Liu, L. Shi, P. An, G. Zhao, J. Kong, X. Wang, X. Meng, J. Zhang, J. Ye, Efficient visible-light-driven carbon dioxide reduction by a single-atom implanted metal-organic framework, Angew. Chem. Int. Ed. 55 (46) (2016) 14310–14314, https://doi.org/10.1002/anie.201608597.
[37] Y. Fu, D. Sun, Y. Chen, R. Huang, Z. Ding, X. Fu, Z. Li, An amine-functionalized titanium metal-organic framework photocatalyst with visible-light-induced activity for CO2 reduction, Angew. Chem. Int. Ed. 51 (14) (2012) 3364–3367, https://doi.org/10.1002/anie.201108357.
[38] R. Li, W. Zhang, K. Zhou, Metal-organic-framework-based catalysts for photoreduction of CO_2, Adv. Mater. 30 (35) (2018) 1705512, https://doi.org/10.1002/adma.201705512.
[39] X.-Y. Dao, J.-H. Guo, X.-Y. Zhang, S.-Q. Wang, X.-M. Cheng, W.-Y. Sun, Structure-dependent iron-based metal-organic frameworks for selective CO_2-to-CH_4 photocatalytic reduction, J. Mater. Chem. A 8 (48) (2020) 25850–25856, https://doi.org/10.1039/D0TA10278D.
[40] C.S. Diercks, S. Lin, N. Kornienko, E.A. Kapustin, E.M. Nichols, C. Zhu, Y. Zhao, C. J. Chang, O.M. Yaghi, Reticular electronic tuning of porphyrin active sites in covalent organic frameworks for electrocatalytic carbon dioxide reduction, J. Am. Chem. Soc. 140 (3) (2018) 1116–1122, https://doi.org/10.1021/jacs.7b11940.
[41] L. Sun, Y. Yuan, F. Wang, Y. Zhao, W. Zhan, X. Han, Selective wet-chemical etching to create TiO_2@MOF frame heterostructure for efficient photocatalytic hydrogen evolution, Nano Energy 74 (2020) 104909, https://doi.org/10.1016/j.nanoen.2020.104909.
[42] H. Dong, X. Zhang, Y. Lu, Y. Yang, Y.-P. Zhang, H.-L. Tang, F.-M. Zhang, Z.-D. Yang, X. Sun, Y. Feng, Regulation of metal ions in smart metal-cluster nodes of metal-organic frameworks with open metal sites for improved photocatalytic CO_2 reduction reaction, Appl. Catal. B: Environ. 276 (2020) 119173, https://doi.org/10.1016/j.apcatb.2020.119173.
[43] D. Yang, H. Yu, T. He, S. Zuo, X. Liu, H. Yang, B. Ni, H. Li, L. Gu, D. Wang, X. Wang, Visible-light-switched electron transfer over single porphyrin-metal atom center for highly selective electroreduction of carbon dioxide, Nat. Commun. 10 (2019) 3844, https://doi.org/10.1038/s41467-019-11817-2.